Molecular mechanism of protein kinase recognition and sorting by the Hsp90 kinome-specific cochaperone Cdc37

Dimitra Keramisanou[a], Adam Aboalroub[a], Ziming Zhang[a], Wenjun Liu[b], Devon Marshall[a], Andrea Diviney[a], Randy W. Larsen[a], Ralf Landgraf[b,c] and Ioannis Gelis[a,*]

[a]Department of Chemistry, University of South Florida, Tampa, FL 33620, USA

[b]Department of Biochemistry and Molecular Biology, University of Miami, Miller School of Medicine, Miami, Florida 33136, United States

[c]Sylvester Comprehensive Cancer Center, University of Miami, Miller School of Medicine, Miami, Florida 33136, United States

*corresponding author: Ioannis Gelis, igelis@usf.edu

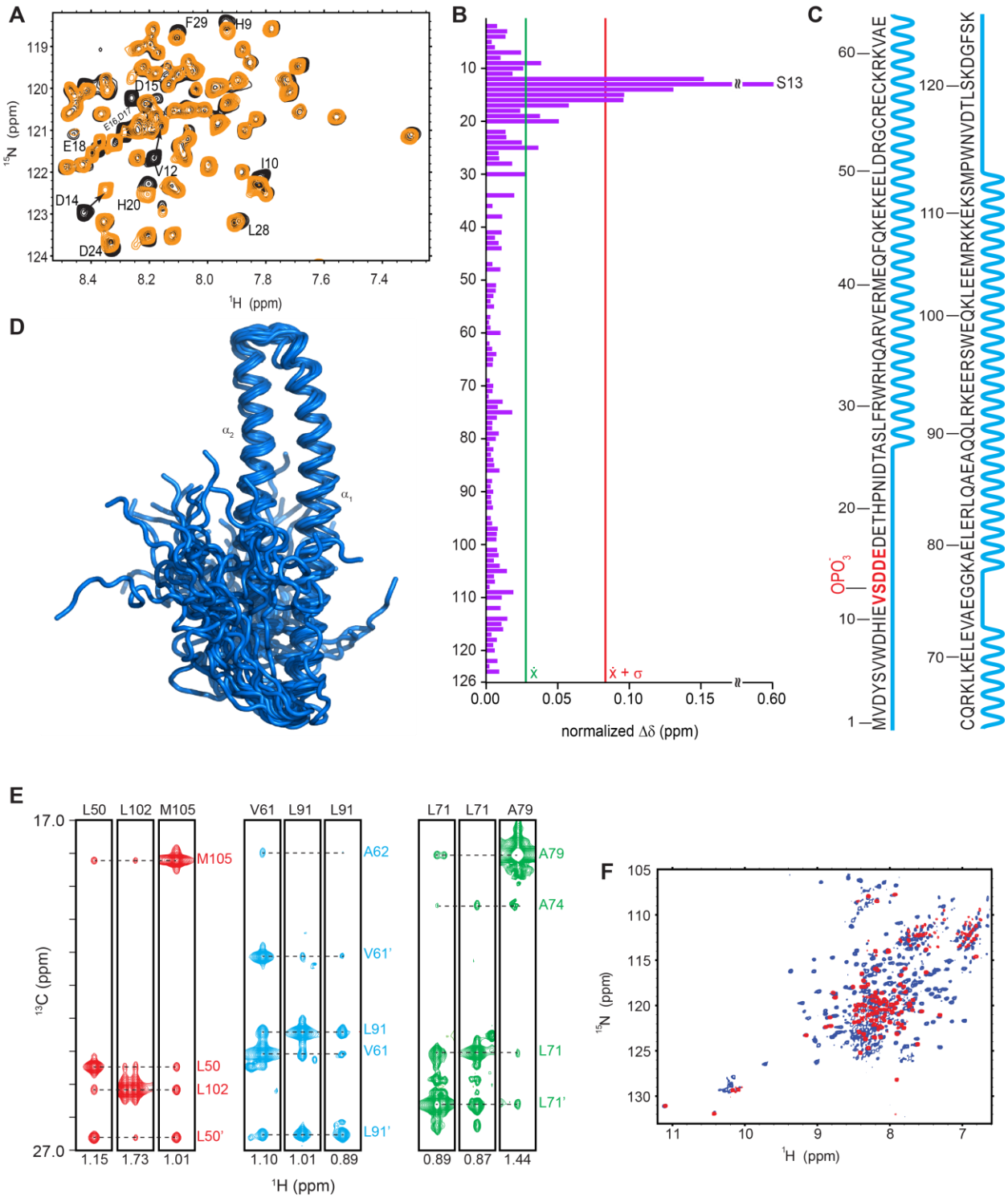

Figure S1: Structural and dynamic properties of N-Cdc37 in solution (Related to Figure 1). (**A**) The central region of the ^{1}H-^{15}N HSQC spectrum of N-Cdc37 in its non-phosphorylated (black) and S13-phosphorylated forms (yellow), showing assignment for residues that exhibit changes in

chemical shift. (**B**) Magnitude of normalized CSP as a function of primary sequence. CSPs greater than the mean or one standard deviation above the mean are marked by green and red lines, respectively. Significant chemical shift perturbations are limited to residues lying adjacent to S13, suggesting that phosphorylation has a highly localized effect, without producing global structural rearrangement on N-Cdc37. It is also noted that phosphorylation has no effect on signal linewidths, indicating that domain dynamics are not affected. (**C**) Secondary structure prediction as a function of the primary sequence, based on the available C_α, C_β, C', N, HN of pN-Cdc37, confirms that S13 phosphorylation does not impact the secondary structure of the domain. The absence of significant CSPs for residues distal to S13 indicates that neither the fold of the domain is affected. (**D**) Structural ensemble of the 20 lowest energy models of N-Cdc37 as determined by a limited set of long range NOEs. A 1.01 pairwise RMSD is obtained for the backbone atoms of the helical-hairpin region (26 - 110). (**E**) A set of selected strips extracted from a three-dimensional HMQC-NOESY-HMQC spectrum of VLIMA-labeled Cdc37 recorded in D_2O at 30^{o}C, showing long range (inter-helical) NOEs for L50, V61 and A79. (**F**) An overlay of the ^{1}H-^{15}N HSQC spectra of full-length Cdc37 (blue) and N-Cdc37 (pink) shows very good peak correspondence suggesting that the overall structure of the domain is not altered due to truncation at the C-terminus.

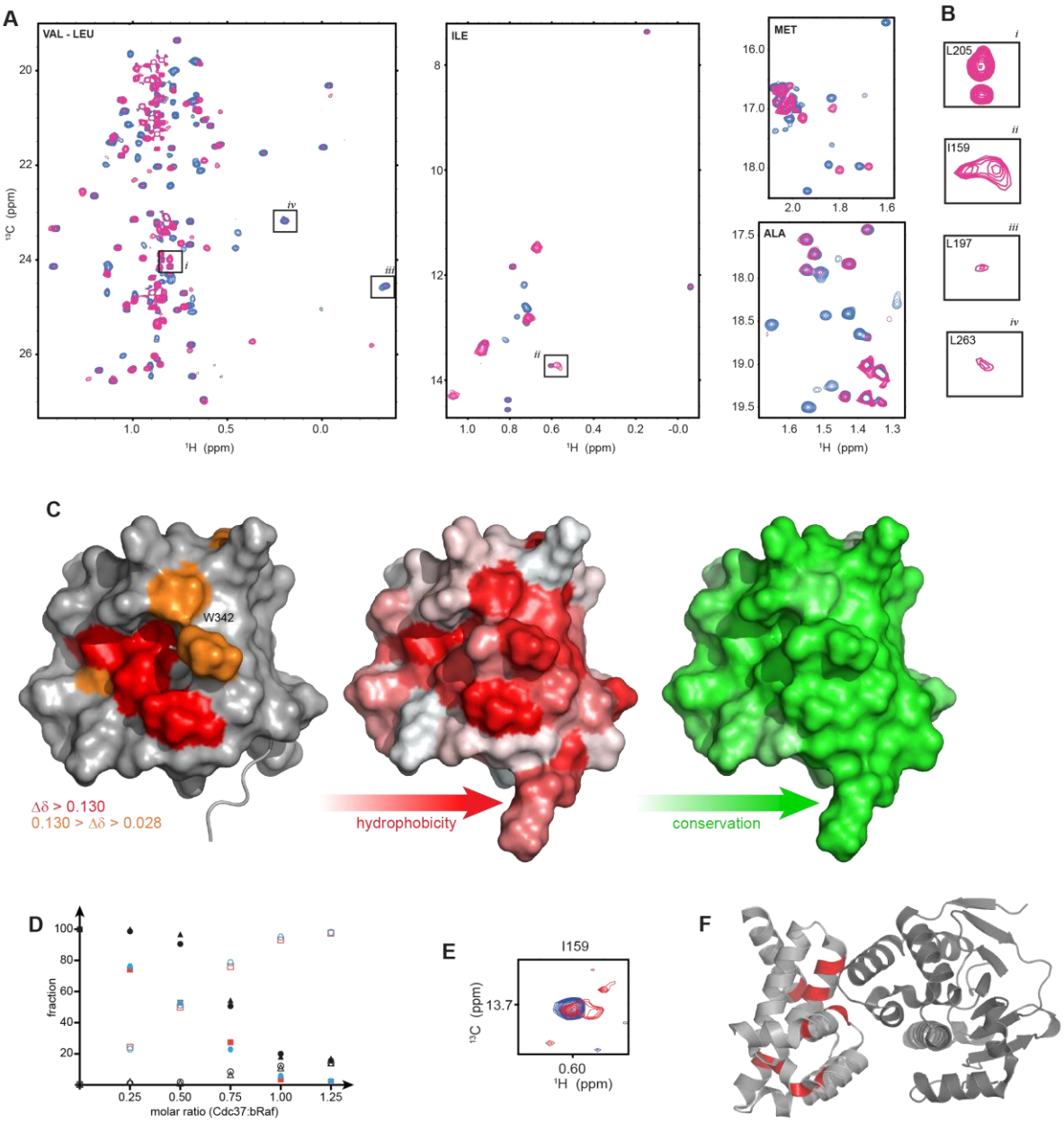

Figure S2: Interaction of Cdc37 with bRaf monitored by Methyl-TROSY NMR (Related to Figure 2). (**A**) Complete ^{1}H-^{13}C HMQC correlation maps of Val/Leu-, Ile-, Met- and Ala-labeled Cdc37 in the absence (blue) or presence of 1.2 equivalents unlabeled bRaf (pink). Boxed regions refer to (b). (**B**) Representative examples of signals from M-Cdc37 methyl groups showing splitting (*i* and *ii*) or extreme line broadening (*iii* and *iv*) in the bound state. (**C**) Left: Surface representation of C-Cdc37 highlighting the methyl groups that experience CSP greater than one standard deviation from the mean (red) and greater than the mean (orange). The position of W342

is also highlighted. Middle and Right: Residue hydrophobicity and conservation, respectively, plotted on the surface of C-Cdc37. In all three cases the same domain orientation as in Figure 2D is used. (**D**) Fraction of free (filled symbols) and bRaf-complexed (open symbols) Cdc37 as a function of Cdc37:bRaf molar ratio, derived by normalizing signal integrals to the signal of the free state. Representative examples from N- (orange), C- (cyan) and M-Cdc37 (black) are shown. For N- and C-Cdc37, at a molar ratio ~1:1, signals of the free-state disappear and a new set of signals reaches a fraction > 90%. For M-Cdc37, the signals affected either become broadened beyond detection and no new signal appears or the signal is split to two broad signals one of which corresponds to the free-state. (**E**) Representative example of an M-Cdc37 signal (I159) showing a pair of broad signals at 1:1 molar ratio, extracted from a spectrum acquired at 7 μM. M-Cdc37 signal splitting and broadening is not a result of self-association of Cdc37-bRaf complexes. (**F**) Structural model of M-Cdc37 (light gray) in complex with N-Hsp90 (dark gray) obtained from 1US7 (Roe et al., 2004). Highlighted in red are M-Cdc37 methyl bearing residues, for which signal splitting is observed in the kinase-bound state.

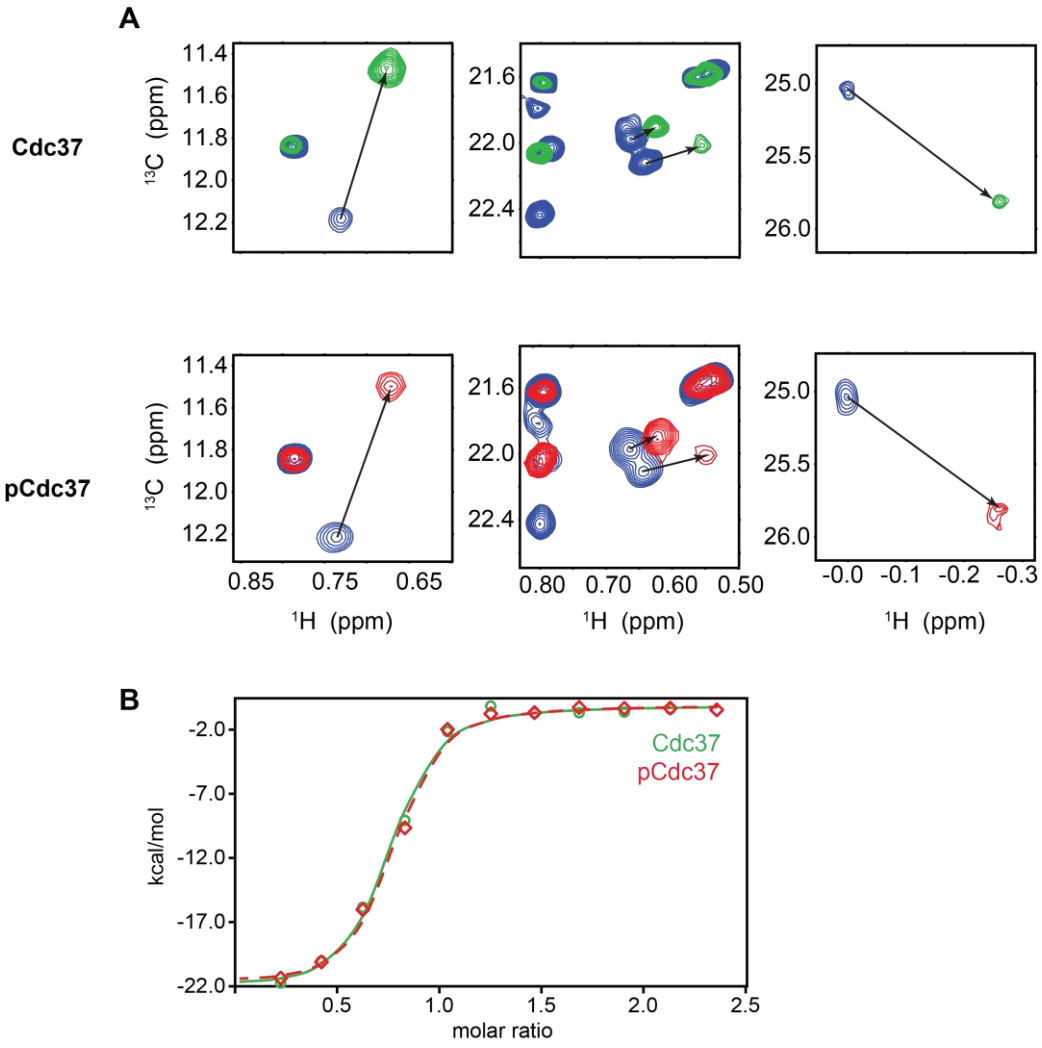

Figure S3: Interaction of bRaf with Cdc37 phosphorylated at S13 (Related to Figure 2). (**A**) Representative examples of methyl signals that experience significant CSP in the presence of bRaf. The panels in the top row were extracted from titrations of non-phosphorylated Cdc37 (blue = free, green = bound) and the panels in the bottom row were extracted from titrations of Cdc37 phosphorylated at S13 (blue = free, red = bound). (**B**) ITC isotherms for the titration of bRaf into non-phosphorylated (green) and phosphorylated Cdc37 (red), yield identical thermodynamic signatures of binding and affinities for both forms.

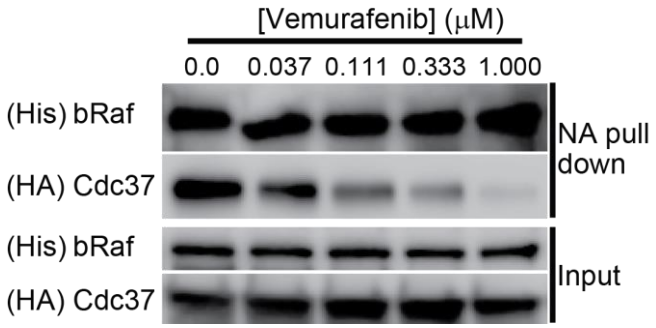

Figure S4: The interaction of bRaf and Cdc37 in pull-down assays is Vemurafenib sensitive (Related to Figure 4). Recombinant bRaf, Cdc37 and BirA were transiently expressed in MCF7. The recovery of Cdc37 after neutravidin pull-down of bRaf is sensitive to Vemurafenib in an inhibitor concentration dependent manner.

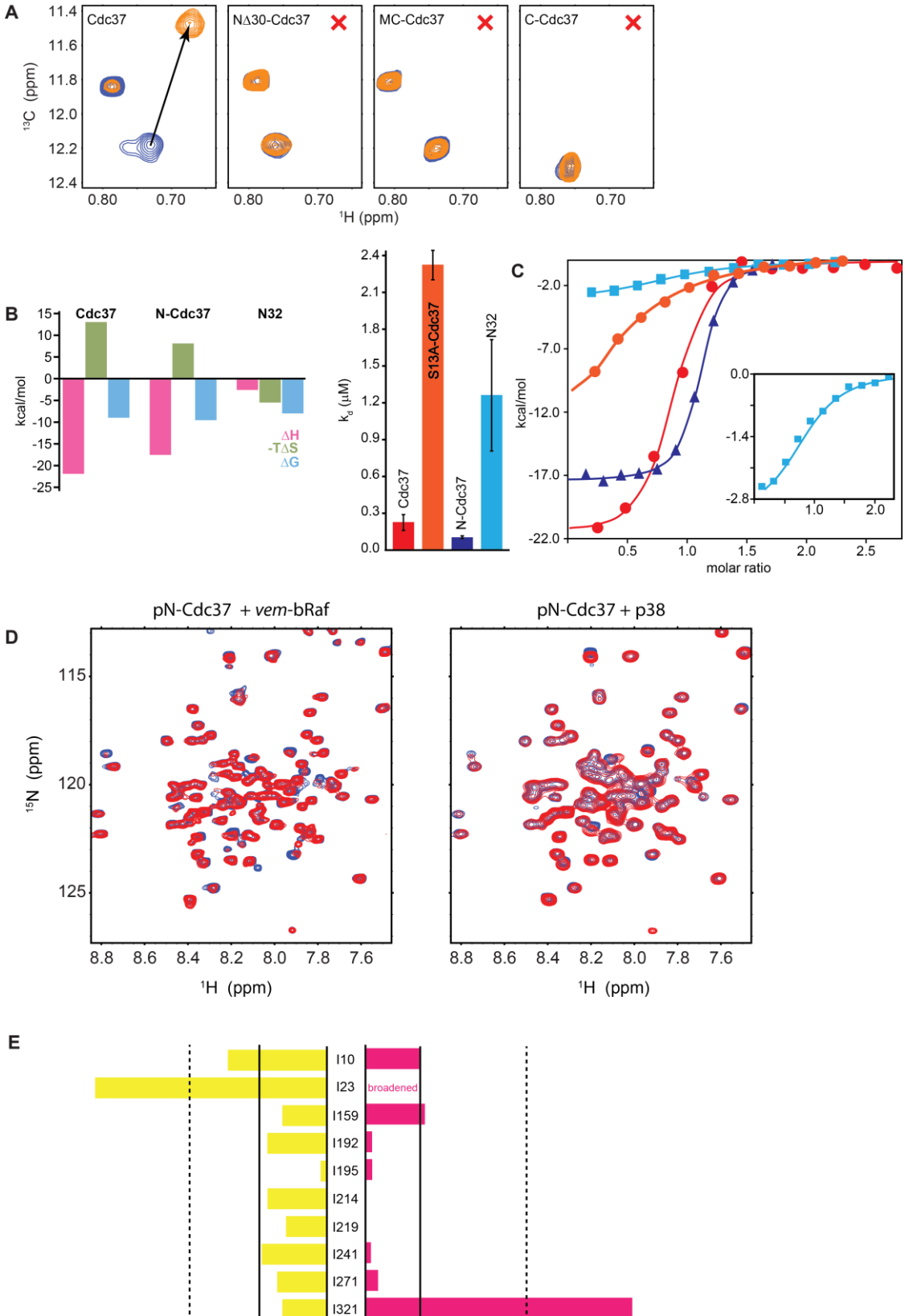
A
Cdc37
NΔ30-Cdc37
MC-Cdc37
C-Cdc37
13C (ppm)
1H (ppm)
B
Cdc37
N-Cdc37
N32
kcal/mol
ΔH
-TΔS
ΔG
S13A-Cdc37
kd (μM)
C
kcal/mol
molar ratio
D
pN-Cdc37 + vem-bRaf
pN-Cdc37 + p38
15N (ppm)
1H (ppm)
E
I10
I23
I159
I192
I195
I214
I219
I241
I271
I321
I337
broadened
normalised Δδ (ppm)

Figure S5: Interaction of Cdc37 constructs with the client and non-client states of bRaf. (Related to Figures 3-6) (**A**) The signal for the $CH_3^{\delta 1}$ group of I321 in the context of full-length Cdc37 (*i*), NΔ30-Cdc37 (*ii*), MC-Cdc37 (*iii*) and C-Cdc37 (*iv*), shown in the absence (blue) or presence (yellow) of bRaf. Only full-length Cdc37 is competent of interacting with the client kinase. (**B**) Thermodynamic signature of bRaf binding to full-length Cdc37, N-Cdc37 and N32 are shown on the left. Dissociation constants derived from ITC are shown on the right, including that for the $Cdc37^{S13A}$ mutant. (**C**) ITC isotherms for the interaction of bRaf with full-length Cdc37 (red), $Cdc37^{S13A}$ (orange), N-Cdc37 (blue) and N32 (cyan). The boxed region shows an expansion of the isotherm obtained for the interaction with N32. (**D**) Central region of the ^{1}H-^{15}N HSQC spectrum of pN-Cdc37 free (blue) or in the presence of a non-client kinase (red). (**E**) CSP pattern for the interaction of Ile-labelled Cdc37 with bRaf and *vem*-bRaf. CSPs greater than the mean or one standard deviation above the mean are marked by continuous and broken lines, respectively.

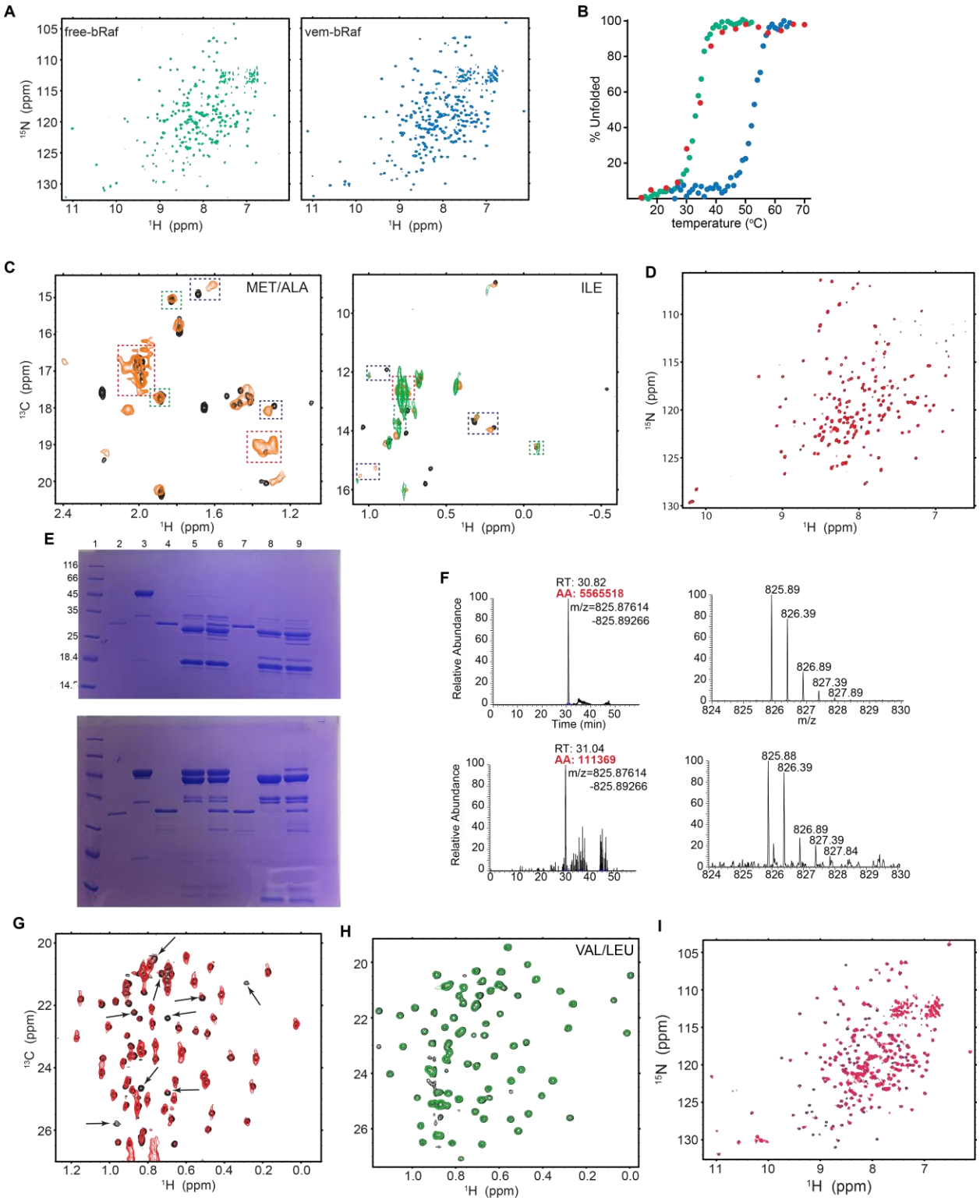

Figure S6: Conformational properties of bRaf and interaction with Cdc37 and Hsp90 (Related to Figure 6). (**A**) The ^{1}H-^{15}N HSQC spectrum of the client state of ^{15}N-labeled bRaf

(green) exhibits excellent signal dispersion and narrow linewidths; however, 60 signals out of the 265 expected are broadened beyond detection. Thus, although the client kinase acquires a near native conformation prior to its engagement with the chaperone machinery, it contains long segment(s) that sample alternate conformations at a ms timescale. Addition of vemurafenib to bRaf (blue) alters the conformational properties of the kinase domain by quenching the slow dynamics observed in the free state (46 new signals appear in the ^{1}H-^{15}N HSQC spectrum of *vem*-bRaf). (**B**) Thermal denaturation curves for free-bRaf (green), free-bRaf^{V600E} (red) and *vem*-braf (blue) determined by molar ellipticity as a function of temperature. No difference in the Tm is observed for bRaf and the mutant bRaf^{V600E}. (**C**) ^{1}H-^{13}C HMQC correlation maps of Ile- (right) and Met/Ala-labeled (left) bRaf in the absence (black) or in the presence of 1.2 equivalents S13-phosphorylated [U-^{2}H]-Cdc37 (yellow). Signals that shift to the unfolded region with narrow linewidths, show a shift, or do not shift are highlighted in red, blue and green boxes, respectively. Similarly to wild-type bRaf, the Ile region of [U-^{2}H]-pCdc37-bound bRaf^{V600E} (green) shows signal clustering in the unfolded region, indicating that, *in vitro*, the oncogenic mutant exhibits the same behavior as wild type bRaf, consistent with the T_m values of the two forms. (**D**) The TROSY ^{1}H-^{15}N HSQC of MC-Cdc37 in the presence of 1.2 equivalents bRaf^{V600E} (red) is superimposable (no chemical shift changes) to that of free-MC-Cdc37 (black) and shows no evidence of line broadening, suggesting that, kinase priming by N-Cdc37 is required for both forms. (**E**) SDS-PAGE of proteolytic digestions of bRaf (lanes 4 and 7), Cdc37 (lanes 5 and 8) and Cdc37-bRaf complex (lanes 6 and 9), using Lys-C (top) and chymotrypsin (bottom), after 30' incubation in ice (lanes 4, 5 and 6) or at 20 ^{o}C (lanes 7, 8 and 9). Free bRaf and Cdc37 are shown for reference in lanes 1 and 2. Free bRaf is relatively resistant to proteolysis by both Lys-C and chymotrypsin, but it becomes susceptible in the presence of Cdc37 and particularly to Lys-C. (**F**) A representative example of enhanced peptide abundance and thus of proteolytic cleavage identified after chymotrypsin digestion at positions 619 and 633, as evident by LC-MS/MS. An enhancement factor of ~50 is observed for Cdc37-bound bRaf (top) over free bRaf (bottom). The manually integrated peak area is highlighted in red. (**G**) The ^{1}H-^{13}C HMQC spectrum of Val/Leu bRaf in the presence of 3.3 equivalents [U-^{2}H]-Hsp90 (monomer:monomer). Arrows show the set of methyl group signals that are affected by the addition of Hsp90 and are common with pCdc37. (**H**) The Val/Leu region of the ^{1}H-^{13}C HMQC spectrum of *vem*-bRaf in the absence (black) or presence of 1.2 equivalents [U-^{2}H]-pCdc37 (green). In contrast to the client state of bRaf, the conformational properties of *vem*-bRaf are significantly altered. (**I**) The TROSY ^{1}H-^{15}N HSQC spectrum of the non-client state of bRaf (blue) shows only small changes in chemical shift and line broadening for a very small number of signals upon addition of pCdc37 (pink).

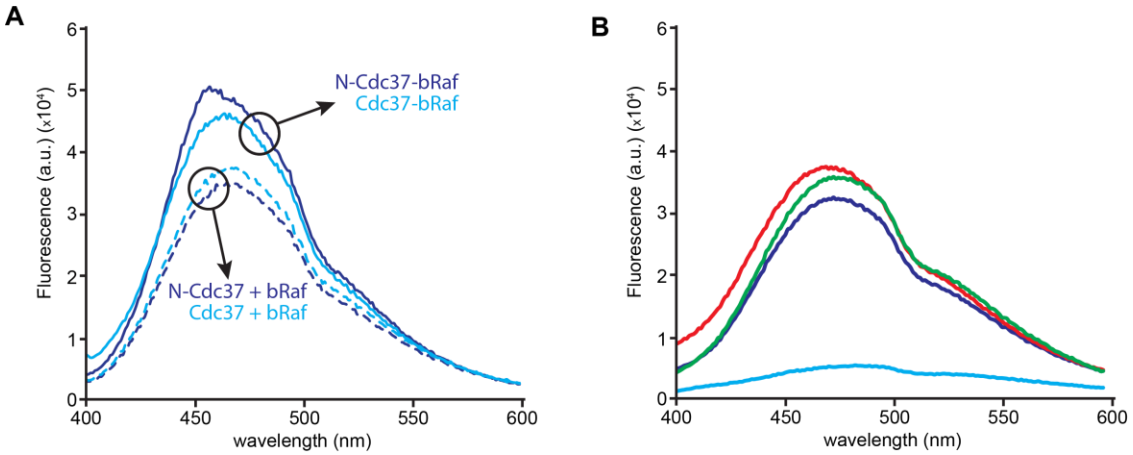

Figure S7: Local bRaf unfolding monitored by emission spectroscopy (Related to Figure 6). (**A**) A comparison between the ANS emission spectra acquired in the presence of bRaf and Cdc37 (cyan-continuous) or bRaf and N-Cdc37 (blue-continuous), to sum the of the spectra acquired in the presence of the corresponding free proteins (broken lines colored as for the complexes). For both cases, the ANS emission intensity in the presence of both bRaf and Cdc37 constructs is significantly higher than the sum of the free proteins. (**B**) Emission spectrum of ANS, in the presence of *vem*-bRaf (blue), Cdc37 (cyan), Cdc37-*vem*-bRaf (red), compared to the sum of the spectra of free proteins (green).

Table S1: NMR structure calculations and statistics for N-Cdc37 (Related to Figure 1)

NMR constraints	
Distance constraints	
Total NOE	350
Short range ($\|i-j\| \leq 1$)	219
Sequential ($\|i-j\| = 1$)	150
Medium-range ($1<\|i-j\|<5$)	111
Long-range ($\|i-j\| > 5$)	20
Hydrogen bonds[a]	142
Total dihedral angle restraints[b]	
ϕ	83
ψ	83
Structure statistics	
Average pairwise r.m.s. deviation[c] *(Å)*	
Backbone	1.01
Heavy	1.71
Ramachandran plot statistics[d]	
Residues in most favorable regions (%)	83.1
Residues in additional favorable regions (%)	16.1
Residues in generously favorable regions (%)	0.8
Residues in disallowed regions (%)	0

[a]Hydrogen bonds were included as both upper and lower limits for two regions of N-Cdc37, spanning a.a. 26-73 and 79-110.

[b]TALOS derived phi and psi dihedral angles were included for the regions 26-72 and 78-125.

[c]RMSD is reported for the 20 lowest energy structures (CYANA target function) of an 200 structures ensemble. Only the a.a. 26-110 was used for the calculation.

[d]Ramachandran statistics were determined using PROCHECK for the complete sequence of N-Cdc37.

DETAILED SUPPLEMENTAL EXPERIMENTAL PROCEDURES

Sample preparations and isotope labeling Full-length human Cdc37 (Cdc37), N-Cdc37 (a.a. 1-126), MC-Cdc37 (a.a. 147-378) and C-Cdc37 (a.a. 288-378) were cloned into a pDB.His.MBP vector (Seiler et al., 2014) to overexpress fusion proteins with an N-terminal, His_6-MBP purification tag, and a TEV cleavage site. The DNA encoding for the catalytic domain of human bRaf, carrying 16 amino acid substitutions, was synthesized for an *E. Coli* optimized codon usage (GeneArt) and cloned into a pDB.His.GST vector (Seiler et al., 2014) to produce a fusion protein with an N-terminal, His_6-GST purification tag, and a TEV cleavage site. NM-Cdc37 was also cloned in the pDB.His.GST vector. A plasmid for the bacterial overexpression of human p38 was obtained from *DNASU Plasmid Repository* (Seiler et al., 2014), encoding for an N-terminal, His-tag, and a TEV cleavage site. Full-length human Hsp90$\alpha\beta$1 was overexpressed from a pET28 plasmid encoding for a His-tag. Cdc37 point mutants were generated using the QuikChange II XL Site-Directed Mutagenesis Kit (Agilent).

Constructs for Cdc37, p38 and Hsp90 were transformed into BL21(DE3) (NEB), and bRaf in TUNER(DE3) (EMD). For the expression of Cdc37 constructs, cells were incubated at 37°C until OD_{600} ~ 0.5 and protein overexpression was induced by the addition of IPTG at a final concentration of 0.5 mM for five hours. p38 was expressed as described previously(Vogtherr et al., 2006). For bRaf overexpression, cells cultures were incubated at 37°C until OD_{600} ~ 0.5 and cooled down into an ice/water bath for 30 minutes. Protein overexpression was induced by the addition of 0.15 mM IPTG at 16ºC and allowed to proceed for 24h. Labeled proteins were expressed in M9 as described above. For the production of double-labeled proteins, media in H_2O were supplemented with $^{15}NH_4Cl$, U-^{13}C6 glucose and trace metals. Uniformly deuterated proteins were expressed in the same way, but in 99.8% D_2O and supplemented with U-^{2}H glucose. Methyl protonated samples were prepared in a perdeuterated background as described previously (Gelis et al., 2007; Sprangers et al., 2007; Tzeng et al., 2012). Briefly, 50 mg/L α-Ketobutyric acid, 100 mg/L α-ketoisovaleric acid, 125 mg/L Met-[^{2}H/$^{13}CH_3$] and 50 mg/L Ala-[^{2}H/$^{13}CH_3$] were added to the media 40 minutes before induction with IPTG. All isotopically labeled chemicals and *bioexpress* media were from CIL. A peptide corresponding to the 32 aminoterminal residues of human Cdc37 was obtained synthetically with a cysteine at position 33 instead of a histidine.

All Cdc37 constructs and p38 were purified as described previously(Vogtherr et al., 2006; Zhang et al., 2015). Cells overexpressing bRaf were resuspended in lysis buffer (50 mM Tris, pH = 8.0, 150 mM NaCl, 10 mM $MgCl_2$, 5 mM 2-mercaptoethanol, 1 mM EDTA, 5% glycerol, 1 mM PMSF and lysozyme) and disrupted by sonication. The lysate was clarified by centrifugation, loaded on a GST column, and washed with lysis buffer, before eluting with 40 mM reduced glutathione in the same buffer. The fusion protein was digested overnight with TEV protease and buffer exchanged into lysis buffer with 20 mM imidazole and 0.2 mM EDTA. GST and TEV were removed over a Ni^{2+}-affinity column and bRaf was run through a Superdex 200 in 50 mM Tris, pH = 8.0, 150 mM NaCl, 5 mM 2-mercaptoethanol, 1 mM EDTA and 5% glycerol. Cells overexpressing Hsp90 were resuspended in 50 mM Tris, pH = 8.0, 1 M NaCl, 20 mM imidazole, 0.2 mM EDTA and 5mM 2-mercaptoethanol. Cells were disrupted by sonication and the lysate was clarified by centrifugation before loading to a Ni^{2+}-affinity column. After extensive washing with lysis buffer the column was washed with 50 mM imidazole and Hsp90 was eluted with the same buffer containing 400 mM imidazole. The protein was further purified over a Superdex 200 in 50 mM Tris, pH = 8.0, 1 M NaCl, 1.0 mM EDTA and 5mM 2-mercaptoethanol.

Cdc37 and N-Cdc37 phosphorylation at position S13 was performed at a protein concentration of ~20 μM, in 25 mM Tris, pH = 7.5, 100 mM KCl, 10 mM $MgCl_2$, 5 mM DTT and 0.5 mM ATP. 2500 units of CKII holoenzyme (NEB) was added, and the reaction was incubated at 30°C overnight. CKII and traces of non-phosphorylated substrate were removed by anion exchange chromatography. In all cases, complete phosphorylation of NMR samples was confirmed by comparing the NMR spectra before and after the phosphorylation reaction.

NMR spectroscopy

All NMR experiments were performed on Varian direct drive 600 and 800 MHz spectrometers equipped with a cryoprobe. Sequential assignment of ^{1}H, ^{13}C, and ^{15}N backbone chemical shifts for N-Cdc37 was achieved by means of through-bond heteronuclear scalar correlations with standard pulse sequences (HNCA, HNCOCA, HNCACB, CBCACONH, HNCO and HNCACO). Selective amino acid labeling (^{15}N-Ala, Gln, His, Cys and $^{15}N/^{13}C$-Lys), unlabeling (Arg, Met) and the acquisition of a 3D HNN experiment (Panchal et al., 2001), further facilitated assignment. Sidechain and methyl group assignment was accomplished with 3D (H)C(CO)NH, 3D H(C)(CO)NH, 3D ^{15}N-edited TOCSY, H(C)CH-TOCSY and (H)CCH-TOCSY. The former three

experiments gave unambiguous assignment for methyl groups of residues in the flexible tails, and for L28, L68 and V73 in the two helix bundle. The remaining methyl groups were assigned using the latter two spectra in combination with side-directed mutagenesis. Methyl group assignment for M-Cdc37 was accomplished using the (H)C(CO)NH and H(C)(CO)NH set of 3D spectra, together with the available backbone assignment(Sreeramulu et al., 2009; Sreeramulu et al., 2005). Full assignment of C-Cdc37 signals has been presented elsewhere (Zhang et al., 2015). All NMR samples for assignments were prepared in 50 mM Hepes, pH = 7.5, 100 mM NaCl, 2.5 mM DTT, with concentrations in the range of 0.3 - 0.5 mM and spectra were recorded at 30°C.

We have investigated the interaction of Cdc37 with protein kinases by monitoring formation of binary Cdc37-kinase complexes using the Methyl-TROSY approach (Gelis et al., 2007; Sprangers and Kay, 2007; Sprangers et al., 2007). Observing methyl resonances allows us to overcome challenges associated with the relatively large molecular weight of the complex (~76 kDa), which in combination with the low temperature range at which experiments are performed (8-20 ^{o}C) and the low concentrations at which the complex is stable over prolonged times (<80 μM) pose serious experimental limitations. Furthermore, the presence of long unstructured segments in both N- and C-Cdc37 results in extensive signal overlap in the central region of the ^{1}H-^{15}N HSQC spectrum of Cdc37, which makes the analysis ambiguous (Supplementary Figure 1F). On the other hand, the methyl groups of Val, Leu, Ile, Met and Ala residues of Cdc37 produce ^{1}H-^{13}C correlation maps of remarkable quality, while they are uniformly distributed throughout the protein structure, and thus are excellent probes to characterize the interaction of the cochaperone with protein kinases (Figure 2). The modular structure of Cdc37 results in good resonance correspondence between spectra of isolated domains or two-domain fragments and the spectra of the full-length protein, which permits the assignment transfer using a domain parsing approach (Figure 2C). Any ambiguities associated with amino acids at or adjacent to linker regions were resolved by acquiring a 3D NOESY spectrum of the full-length Cdc37 or by introducing conservative mutations and thus a nearly complete assignment was obtained (95%). Methyl group assignment transfer from isolated domains to full-length Cdc37 was assisted by a 3D HMQC-NOESY-HMQC spectrum acquired in D_2O and further aided by a series of mutants at linker regions. Assignment at 20^{o}C was obtained by recording several ^{1}H-^{13}C HMQC spectra at different temperatures. All spectra were processed with NMRpipe (Delaglio et al., 1995) and analysed using sparky (T. D. Goddard and D. G. Kneller, SPARKY 3, University of California, San Francisco).

Methyl-TROSY titrations of full-length Cdc37 with bRaf (or *vem*-bRaf) were performed at 20ºC (or 30 ºC), with protein concentrations in the range of 10 to 80 μM. Cdc37-bRaf complexes with $^{2}H/^{13}CH_3$-Cdc37 (IMA- and VL- or VLIMA-labeled) in either of the two phosphorylation states of S13 contained a small molar excess (1.2 equivalents) of unlabeled bRaf and had a final Cdc37 concentration between 60 and 80 μM. Cdc37-bRaf complexes with $^{2}H/^{13}CH_3$-bRaf (VLIMA-labeled) were prepared by the addition of a small molar excess of either S13-phosphorylated [U-^{2}H]-Cdc37 (1.2 equivalents) or [U-^{2}H]-Hsp90 (2.4 equivalents). The final concentration of $^{2}H/^{13}CH_3$-bRaf ranged between 10 and 18 μM. ^{1}H-^{15}N HSQC spectra of ^{15}N-labeled N-Cdc37 in either of the two phosphorylation states of S13, in the presence of the non-client state of bRaf were performed at 30ºC. The concentration of N-Cdc37 varied between 80 and 100 μM and the kinase at the final point was present at three-fold and four-fold excess for *vem*-bRaf and p38, respectively. Combined chemical shift perturbation for the interactions monitored by Methyl-TROSY was calculated according to: $\Delta\delta = \sqrt{\Delta\delta_{^{1}\mathrm{H},i}^{2} + (\Delta\delta_{^{13}\mathrm{C},i} * w_i)^{2}}$, where $\Delta\delta$ is the chemical shift difference between the bound state and the free state in ppm and the weighting factor w_i is set to $\sigma_{H,i}/\sigma_{C,i}$, where σ_i is the standard deviation of deposited chemical shifts at BMRB for that atom. For interactions followed by ^{1}H-^{15}N HSQCs combined chemical shift perturbation was calculated according to: $\Delta\delta = \sqrt{\Delta\delta_{\mathrm{H}}^{2} + \left(\frac{\Delta\delta_{\mathrm{N}}}{5}\right)^{2}}$

Structural model of N-Cdc37 To obtain a three-dimensional model of adequate resolution for functional studies, NOE restraints were derived from a 3D ^{15}N-edited NOESY-HSQC (τ_{mix} = 120 ms), acquired with a fully protonated sample in H_2O, and a 3D HMQC-NOESY-HMQC (τ_{mix} = 250 ms) acquired with a U-$^{2}H/^{12}C$ sample, specifically protonated at the methyl groups of Val, Leu, Ile, Met and Ala, in D_2O. Both spectra were recorded at 30ºC with a sample concentration of 0.4 mM. The structural model was calculated using CYANA 2.1 (Guntert et al., 1997). All NOE distance restraints were manually assigned and only unambiguous pairs of distances were included in the calculations. The C_α, C_β, C', N, HN and H_α NMR chemical shifts served as input for the TALOS-N program (Shen and Bax, 2013) and dihedral angles were extracted and incorporated into the calculations. A set of hydrogen bond restraints was included in the form of upper and lower distance limits for those residues with a predicted helical secondary structure, and only if a strong H_iN-$H_{i+1}N$ NOE was observed. A total of 200 structures were calculated and an ensemble of the

20 lowest energy structures was analyzed. The poor quality of the TOCSY-based spectra for N-Cdc37 has limited the number of unambiguously assigned sidechain resonances for the helical hairpin region, which in turn resulted in a relatively small number of NOEs (Table S1). However, an adequate number of long-range, interhelical NOEs allowed us to obtain a low resolution structural model (b.b. RMSD = 1.01) that is nevertheless very helpful in interpreting functional interactions of the cochaperone with protein kinases.

SEC-MALS Size-exclusion chromatography coupled to multiangle light scattering (MALS) was performed at 20ºC, in 20 mM Tris, pH = 7.5, 100 mM NaCl, 2.0 mM DTT, 0.5 mM EDTA. Protein samples were run through a WTC015S5 column (Wyatt technology) at a flow rate of 0.6 ml/min an detected by UV absorbance. MALS was detected downstream by a miniDAWN TREOS and processed with ASTRA 6. For all samples, the injection volume was 100 μl. Protein concentration for free-Cdc37 and free-bRaf was 49 μM and 34 μM, respectively. Samples containing Cdc37 and bRaf at different molar ratios were prepared by mixing the two proteins at low concentrations (< 10 μM). The volume was subsequently reduced in an amicon stirred cell to obtain Cdc37:bRaf micromolar concentration ratios equal to 80:80 and 80:40.

Immunoprecipitation and pull down MCF7 cells were transfected with kinase clients (ErbB2-bio, bRaf-bio or bRaf^{V600E}-bio), BirA biotinyl transferase (BirA) and, when indicated, HA-Cdc37. The bio-tag on the kinase clients encodes a biotinylation substrate peptide (GLNDIFEAQKIEWHE) for the BirA biotinyl transferase. The lysates were incubated with neutravidin agarose beads (Pierce, 29202) for 1 h. Where indicated, in vitro phosphorylated, *E. coli* expressed Cdc37 was added to the mixture. After the incubation, beads were washed three times with lysis buffer, and associated proteins were analyzed by western blots.

Fluorescence spectroscopy Fluorescence emission of ANS was recorded in 20 mM KPi, pH = 6.8, 100 mM NaCl, 2.5 mM DTT and 0.5 mM EDTA, using an PC1 single photon counting spectrometer (ISS, Inc). The spectra were obtained from 400 to 600 nm, using an excitation wavelength of 290 nm with 1 nm steps and 100 ms integration time. The final ANS concentration

was the same in all samples (16.6 μM), while the concentration of free proteins or of each protein in a mixture was 4.3 μM. Samples were equilibrated for 20 minutes at room temperature prior to data collection.

Isothermal titration calorimetry Titrations were carried out on a VP-ITC calorimeter (GE Healthcare) at 20°C. Protein samples were extensively dialyzed against 20 mM Tris, 100 mM NaCl, 0.5 mM EDTA and 1 mM tris(2-carboxyethyl)phosphine and degassed. For the titrations performed with Cdc37 constructs, the 1429-μl sample cell was filled with the Cdc37 construct at a concentration of ~10 to 12 μM protein (Cdc37, N-Cdc37, MC-Cdc37, C-Cdc37 or NΔ30-Cdc37), and the 281-μl injection syringe was filled with bRaf at 120 - 160 μM. Isotherms for the interaction of bRaf with N32, were measured by titrating N32 (200 μM) into bRaf (18 μM). All titrations included an initial 0.2-μl injection and were carried out by 10 - 12 injections, with a 4 min time interval between each injection. The data were processed with Origin 7.0 (OriginLab Corporation) with the point of the initial injection excluded. Errors in K_d were determined from duplicate measurements.

CD experiments Thermal denaturation of the client and non-client states of bRaf and the extraction of the corresponding melting temperatures was performed by monitoring molar ellipticity at 222 nm, using an AVIV (215) Circular Dichroism Spectrometer. For both states, the concentration of bRaf was 4 μM in 20 mM Tris, pH = 7.5, 100 mM NaCl, 2.5 mM DTT and 0.5 mM EDTA. A small excess of vemurafenib was added for the non-client state (6 μM).

Limited proteolysis and Mass Spectrometry Proteolytic digestions were performed in 20 mM Tris, pH = 7.5, 100 mM NaCl, 2.5 mM DTT and 0.5 mM EDTA. $CaCl_2$ at a final concentration of 10 mM was added for digestion with chymotrypsin. bRaf (5 μM), Cdc37 (30 μM) or a mixture of bRaf and Cdc37 at 5 μM and 30 μM, respectively, were incubated with 1% (w/w) Lys-C or chymotrypsin in ice or at 20 ^{o}C for time intervals ranging between 30’ and five hours. Reaction aliquots were quenched by the addition of formic at a concentration of 5% or by SDS-PAGE loading buffer. Minor changes were observed at different temperatures and thus only reaction

aliquots after 30' incubation at 20 °C were finally analyzed. Reactions were desalted on a C4 column, dried to completeness and resuspended in 0.1 % formic acid for MS analysis. Peptides were separated on a C18 column using an easyNano 1000 (Thermo) and analyzed on a LTQ OrbitrapXL (Thermo), using a top 10 data dependent acquisition. Raw data files were searched using MaxQuant against the sequences of mutant bRaf and wild type Cdc37. Methionine oxidation was included as variable modification and multiple missed cleavages were allowed during the search. The list of bRaf peptides showing enhanced abundance in the presence of Cdc37 (Figure 6B) is provided below.

peptide	unique	enhancement factor
Lys-C		
^{484}MLNVTAPTPQQLQAFKNEVGVLRK^{507}	no	1.3
^{484}MLNVTAPTPQQLQAFK^{499}	yes	×
^{500}NEVGVLRK^{507}	yes	×
^{548}FEMKKLIDIARQTARGMDYLHAK^{570}	yes	×
^{552}KLIDIARQTARGMDYLHAK^{570}	no	4.7
^{553}LIDIARQTARGMDYLHAK^{570}	no	3.3
^{571}SIIHRDLKSNNIFLHEDNTVKIGDFGLATVK^{601}	no	12.0
^{579}SNNIFLHEDNTVKIGDFGLATVK^{591}	no	11.7
^{592}IGDFGLATVK^{601}	no	1.4
^{700}KRDERPSFPRILAEIEELARELSG^{723}	no	810.0
^{701}RDERPSFPRILAEIEELARELSG^{723}	yes	×
chymotrypsin		
^{473}KGKWHGDVAVKMLNVTAPTPQQLQAF^{498}	no	2.5
^{499}KNEVGVLRKTRHVNILLFMGY^{519}	no	72.0
^{499}KNEVGVLRKTRHVNILLF^{516}	yes	×
^{517}MGYSTKPQLAIVTQW^{531}	no	9.8
^{520}STKPQLAIVTQW^{531}	no	3.2
^{539}HHLHASETKF^{548}	yes	×
^{605}SGSHQFEQLSGSILWMAPEVIRMQDSNPY^{633}	yes	×
^{605}SGSHQFEQLSGSILW^{619}	no	7.4
^{620}MAPEVIRMQDSNPYSFQSDVY^{640}	no	90
^{620}MAPEVIRMQDSNPY^{633}	no	49.9
^{634}SFQSDVY^{640}	yes	×
^{648}ELMTGQLPY^{656}	yes	×

Supplemental References

Delaglio, F., Grzesiek, S., Vuister, G.W., Zhu, G., Pfeifer, J., and Bax, A. (1995). NMRPipe: a multidimensional spectral processing system based on UNIX pipes. Journal of biomolecular NMR *6*, 277-293.

Gelis, I., Bonvin, A.M., Keramisanou, D., Koukaki, M., Gouridis, G., Karamanou, S., Economou, A., and Kalodimos, C.G. (2007). Structural basis for signal-sequence recognition by the translocase motor SecA as determined by NMR. Cell *131*, 756-769.

Guntert, P., Mumenthaler, C., and Wuthrich, K. (1997). Torsion angle dynamics for NMR structure calculation with the new program DYANA. Journal of molecular biology *273*, 283-298.

Panchal, S.C., Bhavesh, N.S., and Hosur, R.V. (2001). Improved 3D triple resonance experiments, HNN and HN(C)N, for HN and 15N sequential correlations in (13C, 15N) labeled proteins: application to unfolded proteins. Journal of biomolecular NMR *20*, 135-147.

Roe, S.M., Ali, M.M., Meyer, P., Vaughan, C.K., Panaretou, B., Piper, P.W., Prodromou, C., and Pearl, L.H. (2004). The Mechanism of Hsp90 regulation by the protein kinase-specific cochaperone p50(cdc37). Cell *116*, 87-98.

Seiler, C.Y., Park, J.G., Sharma, A., Hunter, P., Surapaneni, P., Sedillo, C., Field, J., Algar, R., Price, A., Steel, J*., et al.* (2014). DNASU plasmid and PSI:Biology-Materials repositories: resources to accelerate biological research. Nucleic acids research *42*, D1253-1260.

Shen, Y., and Bax, A. (2013). Protein backbone and sidechain torsion angles predicted from NMR chemical shifts using artificial neural networks. Journal of biomolecular NMR *56*, 227-241.

Sprangers, R., and Kay, L.E. (2007). Quantitative dynamics and binding studies of the 20S proteasome by NMR. Nature *445*, 618-622.

Sprangers, R., Velyvis, A., and Kay, L.E. (2007). Solution NMR of supramolecular complexes: providing new insights into function. Nature methods *4*, 697-703.

Sreeramulu, S., Jonker, H.R., Langer, T., Richter, C., Lancaster, C.R., and Schwalbe, H. (2009). The human Cdc37.Hsp90 complex studied by heteronuclear NMR spectroscopy. The Journal of biological chemistry *284*, 3885-3896.

Sreeramulu, S., Kumar, J., Richter, C., Vogtherr, M., Saxena, K., Langer, T., and Schwalbe, H. (2005). 1H, 13C and 15N backbone resonance assignment of the Hsp90 binding domain of human Cdc37. Journal of biomolecular NMR *32*, 262.

Tzeng, S.R., Pai, M.T., and Kalodimos, C.G. (2012). NMR studies of large protein systems. Methods in molecular biology *831*, 133-140.

Vogtherr, M., Saxena, K., Hoelder, S., Grimme, S., Betz, M., Schieborr, U., Pescatore, B., Robin, M., Delarbre, L., Langer, T*., et al.* (2006). NMR characterization of kinase p38 dynamics in free and ligand-bound forms. Angewandte Chemie *45*, 993-997.

Zhang, Z., Keramisanou, D., Dudhat, A., Pare, M., and Gelis, I. (2015). The C-terminal domain of human Cdc37 studied by solution NMR. Journal of biomolecular NMR.